J. Membrane Biol. 48, 115–139 (1979)

Further Evidence for the Parallel Pathway Model of the Metabolic Control of the Electrogenic Pump in *Nitella* as Obtained from the High Frequency Slope of the Action of Light

Jürgen Martens, Ulf-Peter Hansen, and Jens Warncke

Institut für Angewandte Physik, Neue Universität, Haus N 61 A, 23 Kiel, West Germany

Received 1 December 1978

Summary. Previous investigations of the frequency response of the action of light on the membrane potential in *Nitella* have revealed 5 time constants and 3 zeros in the range of 2 sec to 20 min. Now, the frequency range is extended by means of filter and correlation techniques to its upper theoretical limit of about 20 Hz. Thus the number of experimentally accessible time constants is increased from 5 to 8, the number of the zeros from 3 to 5. The time constant at 0.01 sec is shown to originate from the electrical impedance of the membrane. The other 7 time constants are labels for the reactions mediating the light effect, and the zeros provide information about the arrangement of these reactions. The new results support and extend the basic concept proposed by Hansen (Hansen, U.-P. 1978; *J. Membrane Biol.* **41**: 197) that light acts via three parallel pathways on membrane potential. This model predicts two essential parameters obtained from the high-frequency measurements correctly from the data gained at low frequencies and is capable of reducing the great variety of measured curve shapes of the frequency responses to much smaller changes in two basic parameters.

During the last years there has been rapid progress in the investigation of the mechanisms of transmembrane transport. However, less is known about the adjustment of this transport to the requirements of the metabolism in the cell. Whereas in the field of transport mechanisms biochemistry of the "pumps" and "channels" is already under investigation, research in the field of metabolic control of transport across the plasma membrane is still in the first stage, the phenomenological approach.

A problem of this kind is the action of light on the membrane potential in green plant cells. In this case we are concerned with the interaction of spatially separated functional units, i.e., photosynthesis in the chloroplasts and ion transport at the plasmalemma. An advanced stage of the phenomenological approach is the creation of mathemati-

0022-2631/79/0048-0115/$05.00

cally tractable models. The benefits of mathematically tractable models are that the investigator is obliged to think precisely about his premises and his experiments, that these models have a conceptual function in focussing attention on basic properties, and that they can be tested quantitatively by checking the predictions to be made of the behavior of the system under new conditions.

In the case of light-induced changes in membrane potential of *Nitella*, Hansen (1974, 1978) has shown that system theory based on reaction kinetics is a means of creating such a mathematically tractable model. The crucial data of this model are the time constants which are supposed to label the reaction steps in the chain of reactants mediating the light effect on the membrane potential. By means of these time constants we can keep track of the labeled reactions, if the system is subjected to different experimental conditions.

The number of time constants provided by that method depends on the range of the time scale employed in the experiments. In the previous experiments (Hansen, 1974; 1978) six time constants were found in the range of 0.2 sec to 20 min. Due to the better resolution provided by sine waves, the measurements were done in the frequency domain with frequencies ranging from 0.5 to 6.7×10^{-5} Hz (1 cycle/4 hr). The determination of shorter time constants was limited by the decrease of the amplitude of the light-induced signals at higher frequencies. They became hidden in the noise at a magnitude of 30 μV.

In the experiments reported here, additional time constants were found by extending the frequency range by means of filter and correlation techniques.

Hansen (1978) arranged the time constants in a model assuming that light acts on membrane potential via three parallel pathways. According to the properties of mathematically tractable models quoted above, it will be shown that the concept of three parallel pathways is supported by the new measurements, because it predicts two basic coefficients gained from the new measurements correctly.

Materials and Methods

General

Nitella mucronata (A. Braun) Miquel was grown in Medium *II* proposed by Forsberg (1965) at 17 °C and 16 hr light per day at an intensity of 1 W m^{-2}.

During the experiments an isolated internodal cell of *Nitella* was placed in a Lucite vessel containing 25 ml of the following bathing medium: KCl, 0.1 mM; NaCl, 1.0 mM;

$CaCl_2$, 0.1 mM. The pH was unbuffered. Perfusion had to be stopped during the experiments because it caused too much noise. Thus the constancy of the kinetic behavior had to be tested during the experiments by repeating the measurements at some frequencies. The temperature was 25 to 27 °C.

Light Intensity

The light intensity, i, of a red luminescence diode MV4H of Monsanto was modulated by means of a digital sine-wave generator (Hansen, 1970)

$$i_{(t)} = i_m + I_o \sin \omega t \tag{1}$$

with i_m being the mean value of the light intensity of 1 Wm^{-2}, I_o the amplitude of the modulation (0.6 Wm^{-2}), and $\omega = 2\pi f$, the angular frequency.

The insertion of the microelectrode was done at higher light intensity (10 Wm^{-2}, white light). Before the experiments started, the cell was kept in the red light for several hours.

Recording Apparatus

Since signals in the order of nanovolts had to be measured, extreme care had to be applied in order to prevent picking up spurious signals. As shown in Fig. 1, the membrane potential was measured by a microelectrode inserted into the vacuole and by a reference electrode positioned outside the cell near the inserted microelectrode. Both electrodes were mounted on the same manipulator and surrounded by the same screening tube, and were connected to the inputs of a FET-differential amplifier.

The microelectrode had a tip diameter of about 1 μm and was filled with 1 N KCl. The reference electrode was a microelectrode with a broken tip filled with 1 N KCl agar. Since it was a little shorter than the microelectrode, it stayed outside when the microelectrode penetrated into the vacuole. A separate Ag/AgCl electrode provided the grounding of the bathing medium via a 1 N KCl agar bridge.

Figure 1 shows that the absolute value and the changes of membrane potential caused by changes of light intensity with frequencies lower than 0.13 Hz were displayed on two traces of a chart recorder, as described in a previous paper (Hansen, Warncke & Keunecke, 1973). From these records the amplitudes and the phase shifts of the light-induced changes were evaluated by hand.

Since even shielded cables picked up too much spurious signals in the submicrovolt region, the small signals due to higher frequencies were branched off from the pathway of the lower frequencies via a CR high-pass filter ($\tau = 130$ sec), and amplified by a factor of 2000 by means of a second amplifier mounted on the manipulator. Because the high-frequency signals were hidden in the noise, they had to be treated by filter and correlation techniques.

Detection of Noisy Signals by Means of Cross-Correlation

The desired parameters—amplitude A_o and phase shift φ—of a signal which is heavily corrupted with noise can be determined by means of band-pass filters or by means of correlators. The employed method of cross-correlation is described in *Appendix I*. Briefly, the noisy signals are multiplied with the input signal [light intensity, *see* Eq. (1)], and the product is integrated over time, resulting in the ramp functions shown in inset *B*

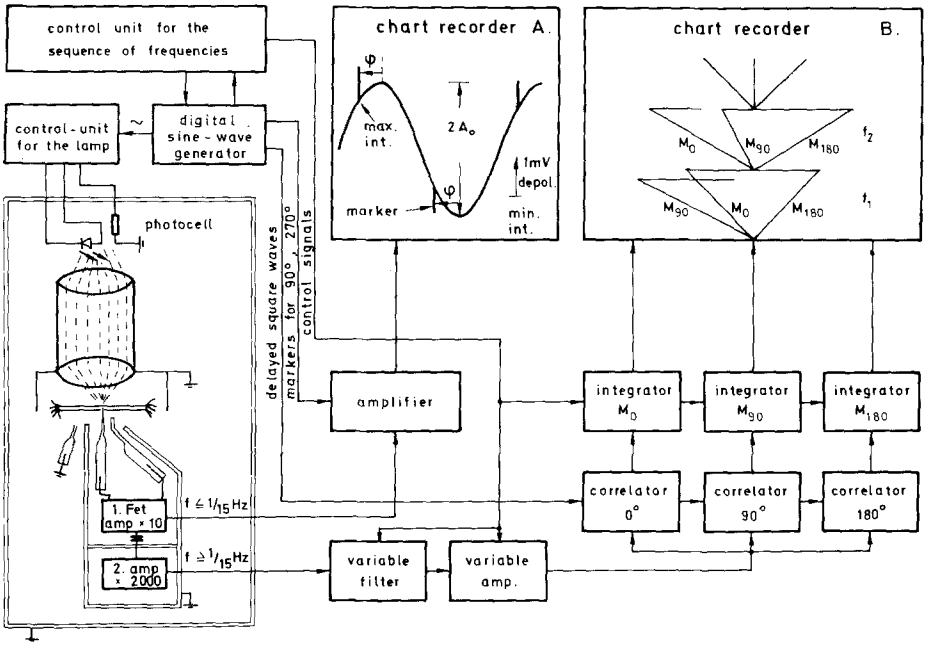

Fig. 1. The experimental set-up. The sinusoidal light-induced signals with frequencies lower than 1/15 Hz are displayed directly on chart recorder *A*. The signals caused by higher frequencies are evaluated by means of correlation techniques and are determined from the output of the integrators on chart recorder *B* by means of Eqs. (A6) and (A7)

of Fig. 1. Two correlators are required in order to determine the amplitudes A_o and the phase shifts φ [*see* Eqs. (A6) and (A7)].

A third correlator was employed as a test for malfunctions. Since its reference signal was delayed by 180°, its output signal M_{180} should be the negative value of M_o.

The required minimum correlation times T [*see* Eq. (A3)] for a desired signal to noise ratio Q of 10 have been calculated by means of Eq. (A12) for two extreme frequency responses and for the frequency response of a "mean *Nitella*", and are displayed in Table 1. The noise-power spectrum $sn_{(f)}$ is given by the $1/f$ noise with a mean value of $5(\mu V)^2$ sec at 1 Hz (Warncke, 1974; Grahn, 1978). The $1/f^2$ component of the noise may be neglected because it merges into the $1/f$ noise at frequencies between 1 and 0.1 Hz (Korff, 1979). Also the influence of the electrical membrane impedance resulting in the time constant τ_8 is not taken into account, since it acts on the noise and on the light-induced signal in the same manner.

The most important conclusion to be drawn from the data in Table 1 is that, depending on the individual cell, for frequencies higher than 4 to 32 Hz measurements cannot be made, whatever technique is employed, because T gets too long (up to 10^8 min).

Filtering

The signal from the plasma membrane has to pass a band-pass filter, tuned to the applied frequency, before entering the correlators. The main purpose of this filter is to reduce the magnitude of the noise by narrowing the bandwidth in order to prevent

Table 1. Required correlation times T for a desired signal to noise ratio Q = 10 (*see* Eq. (A 12))[a]

f [Hz]	$sn_{(f)}$ (μV^2 sec)	A (small signal)		B (strong signal)		C (mean cell)		T_{act} (min)	Amp	Dark test % of mean cell
		A_o (μV)	T (min)	A_o (μV)	T (min)	A_o (μV)	T (min)			
1	5	3.6	4 sec	22		3.5	4 sec	10	2×10^5	1.5
2	2.5	0.47	1.9	11		0.5	1.6	30	2×10^5	6
4	1.3	0.046	99	3.6	1 sec	0.29	2.5	30	6×10^5	5
8	0.63	0.0040	63	0.87	8 sec	0.1	11	120	10^6	5
16	0.31	0.00039	3.4×10^5	0.16	2	0.028	66	120	10^6	15
32	0.15	0.00004	1.6×10^7	0.022	57	0.0074	457			
64	0.075	0.00001	1.3×10^8	0.0029	1486	0.0014	6378			

[a] The evaluation of the amplitudes A_o of the light-induced signals was based on Eq. (5) making use of the kinetic constants displayed in Table 2. (*A*): Cell No. 4 (*see* Table 2) gave the smallest signal. (*B*): Cell No. 7 exhibited the largest signal. (*C*): A hypothetical "mean *Nitella*" was composed from the mean values displayed in Table 2. In column "T_{act}" the actually applied integration times are shown. The column "dark test" gives the deflections of the integrators when the alga was shielded against the light by black paper.

overload of the amplifiers and of the correlators. In the case of white noise this filtering does not reduce the required correlation time because the time constant of internal correlation [*see* Eqs. (A9) and (A10)] is increased by narrowing the bandwidth. However, in the case of the pink $1/f$ or $1/f^2$ noise in *Nitella* (Warncke, 1974; Korff, 1979) it is an advantage to get rid of the excess noise at low frequencies.

Technical Details

The complete recording apparatus for high frequencies is shown in Fig. 1. It consists of the FET preamplifier ($\times 10$), the ac amplifier ($\times 2000$), the filter ($\times 1$) tuned to the applied frequency f_o, a third amplifier with variable amplification ($\times 1$ to $\times 50$, *see* column *amp* in Table 1), and three correlators in parallel, consisting of a multiplier, an integrator, and a trace on chart recorder B, each. The bandwidth Δf of the filter is $f_o/8$. A smaller bandwidth is not useful, because in that case oscillations caused by peaks of the noise signal would damp out too slowly.

The amplification of the third amplifier, the frequency f_o of the band-pass filter, and the capacitors of the integrators were set automatically by a control unit connected to the frequency coder of the digital sine-wave generator. It also determined the integration times, zeroed the integrators at the beginning of an integration period, and switched the frequency coder of the sine-wave generator to the next frequency. Thus the whole frequency response could be measured without manual interference after inserting the microelectrode and after pushing the start button.

The reference signals of the correlators were not sine waves, but square waves in phase with the sine or cosine wave, since the square waves could be generated more easily from the phase counter of the digital sine wave generator (Hansen, 1970) and because the multipliers were much easier built, if square waves were used as reference signals.

Reliability Tests

The indirect measurement of signals in the range of nanovolts is very sensitive to spurious signals like those transmitted from the current driving the luminescence diode. Thus it was tested whether there was any deflection of M_o or M_{90} [*see* Eqs. (A4) and (A5)] when the light of the diode was screened by black paper. These tests led to the demand of enlarging the distance between the alga and the diode by using a pair of lenses mounted in a grounded metal tube and of shielding the electrodes down to the surface of the bathing medium. Of course, wiring and grounding of the whole set-up had to be done by extreme care and had to be controlled by repeated tests (*see* last column in Table 1).

Long term integration may suffer from drift, which may originate from the cell or the electronic apparatus. Drift would act on all three correlators in the same manner, and thus would disturb the balance

$$M_o = -M_{180}. \tag{2}$$

Results

Linearity

A condition *sine qua non* for the approach presented here is linearity. Thus the range of linearity had to be checked. Single internodal cells of

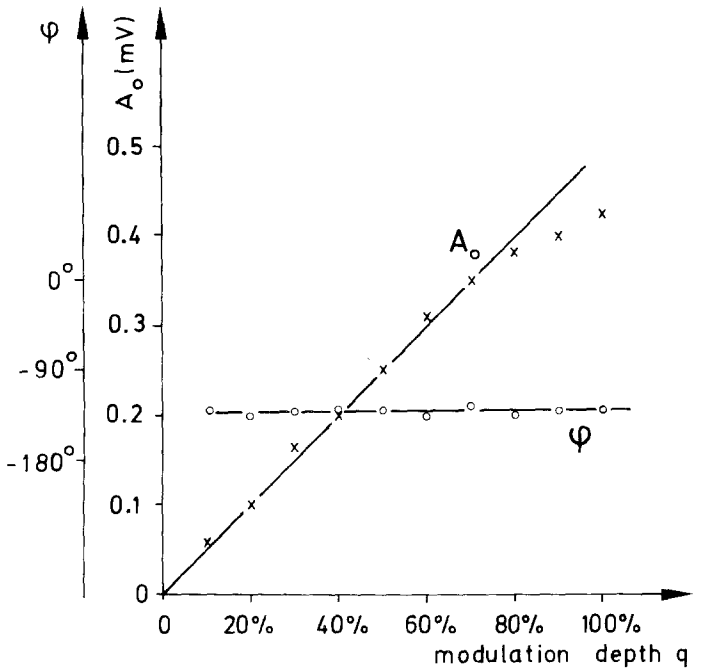

Fig. 2. A test for linearity at a frequency of 1/15 Hz, which shows that linearity holds up to a modulation depth [*see* Eq. (3)] of about 80 %. Mean value of the intensity of the red light: 1 W/m^2. Temperature: 25 to 27 °C

Nitella were illuminated with sinusoidally modulated light intensity and the modulation depth [*see* Eq. (1)]

$$q=\frac{I_o}{i_m} \tag{3}$$

was varied.

Figure 2 displays the result of such an experiment performed at a frequency of 15 cycles/sec (0.67 Hz). The amplitude A_o and the phase shifts φ of the light-induced changes in the membrane potential are plotted *vs.* the modulation depth q. It is seen that linearity holds up to $q=80\,\%$. This is indicated by the amplitude increasing in straight-line proportion to q and by the independence of the phase on q.

The situation was found to be even better at the smaller signals of higher frequencies. Using a modulation depth of $q=60\,\%$ in the following experiments ensured that the requirement of linearity was met.

Measurement of the Frequency Responses

The insets of Fig. 1 demonstrate the two basic concepts used for the evaluation of the light-induced responses of the membrane potential in

Nitella. At low frequencies (0.13 to 1.4×10^{-4} Hz) the sinusoidal changes in membrane potential caused by the sinusoidal modulation of the light intensity [*see* Eq. (1)] were recorded and the amplitudes A_o and the phase shifts φ were determined directly in the records (*see* Fig. 1, inset *A*).

At higher frequencies (0.13 to 16 Hz) the correlation technique described above was employed. M_0, M_{90}, and M_{180} [*see* Eqs. (A4) and (A5)] were determined from the slopes of the ramp functions shown in inset *B* of Fig. 1. These ramp functions are the outputs of the integrators. The amplitudes A_o and the phases φ were calculated by means of Eqs. (A6) and (A7).

Each determination of A_o and of φ by one of the above methods resulted in a dot in the frequency response of the amplitude and in one dot in the frequency response of the phase, as in Fig. 3.

Different types of frequency responses were found. Two examples are given in Fig. 3, Nos. 4 and 7. Common to all of them is the decrease of the amplitude and the increase of the phase delay with increasing frequency. In Fig. 3, No. 7, a notch is seen; that is a region where the phase shift exhibits a rapid change within a limited range of frequencies and the amplitude displays something like a "valley". No notch is seen in No. 4. This variety in the results is not caused by experimental error. In the discussion it will be shown that it is a typical feature of the proposed model.

Evaluation of the Time-Constants

As postulated by the theory of reaction kinetics (*see Appendix II* and Hansen, 1978) and as illustrated in the discussion, frequency responses $H_{(jf)}$ like those displayed in Fig. 3 have to be fitted by a special class of mathematical functions, which is represented by Eq. (4).

$$H_{(jf)} = \frac{N_{(jf)}}{D_{(jf)}} \tag{4}$$

with $N_{(jf)}$ and $D_{(jf)}$ being polynomials of the frequency f. $j = \sqrt{-1}$ is the imaginary unit. $N_{(jf)}$ and $D_{(jf)}$ can be factorized.

$$H_{(jf)} = H_s \frac{(1 - p n_4)(1 - p n_5)}{(1 - p\tau_4)(1 - p\tau_5)(1 - p\tau_6)(1 - p\tau_7)(1 - p\tau_8)} \tag{5}$$

with $p = 2\pi jf$ and H_s being the "dc amplification". The numbers of the roots of the numerator $N_{(jf)}$(n_i, called the "inverse zeros") and of the

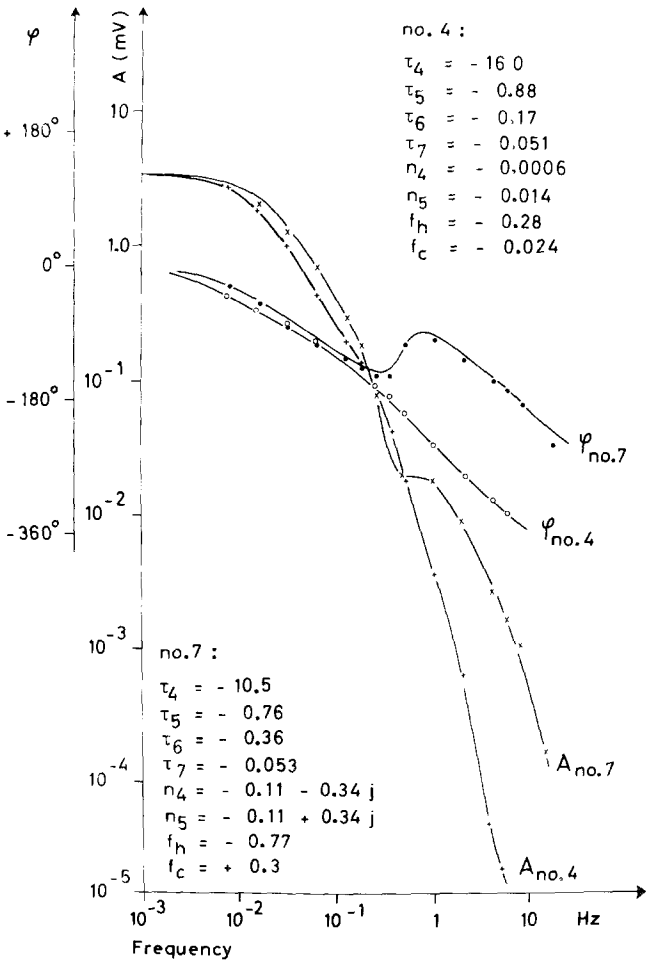

Fig. 3. Two different types of measured frequency responses of the action of light on membrane potential obtained from cell No. 4 and cell No. 7 in Table 2. Red light, intensity 1 W/m², temperature: 25 to 27 °C

roots of the denominator $D_{(jf)}$ (τ_i, called the "time constants" or the "inverse poles") are different in different systems, and have to be determined by curve-fitting routines. In Eq. (5) indices are used which are consistent with the nomenclature started by Hansen (1978).

Without the aid of a computer the following features can be seen from the frequency responses displayed in Fig. 3:

a) The notch of No. 7 requires a pair of conjugate complex zeros (*see* n_4 and n_5 in Table 2). Thus the degree m of $N_{(jf)}$ – that is the number of brackets in the numerator in Eq. (5) – has to be 2 at least.

Table 2. The kinetic data of Eq. (5) and of Eq. (14) obtained at 25 to 27 °C at a medium intensity i_m [*see* Eq. (1)] of the red light of about 1 W/m^2[a]

No. of cell	H_s μV/%	τ_4	τ_5	τ_6	τ_7	τ_8	n_4 and n_5	h_h	h_c
		sec							
1	46	−5.2	−0.84	−0.11	−0.021	−0.0019	−0.012 +/−0.032j	−0.15	0.012
2	64	−10.5	−0.70	−0.16	−0.032	−0.0066	0.016 +/−0.018j	−0.32	0.022
3	144	−23.0	−0.73	−0.42	−0.088	−0.021	−0.17 +/−0.32j	−0.78	0.25
4	92	−16.0	−0.88	−0.17	−0.051	−0.0003	−0.0006 0.014	−0.28	0.024
5	108	−13.4	−0.89	−0.29	−0.037	−0.023	0.0014 +/−0.026j	−0.36	0.007
6	48	−11.5	−1.15	−0.57	−0.006	−0.0029	−0.30 0.031	−0.33	−0.011
7	90	−10.5	−0.76	−0.35	−0.053	−0.013	−0.11 +/−0.34j	−0.77	0.31
8	54	−7.5	−0.86	−0.09	−0.031	−0.031	−0.010 +/−0.027j	−0.14	0.022
9	54	−8.6	−0.78	−0.11	−0.078	−0.048	−0.024 +/−0.054j	−0.44	0.26
10	50	−5.7	−0.74	−0.11	−0.023	−0.020	−0.012 +/−0.031j	−0.16	0.015
Mean values	70	−10.2	−0.83	−0.20	−0.034	−0.0086	−0.03 +/−0.074j	−0.31	0.035
Variance (factor)	1.5	1.5	1.2	1.9	2.1	4.3	3.4 3.3	1.7	4.0

[a] n_4 and n_5 were found to be real numbers as well as a pair of conjugate complex numbers. The second case is indicated by the "+/−" sign and the unit $j=\sqrt{-1}$. For the calculation of the mean values of n_4/n_5 only the complex zeros with negative real components were used. The variance σ is given as a factor. The unit of the τ_i and n_i is sec.

b) In most of the measured frequency responses the slope at high frequencies approaches f^{-r}, with $r=3$. Considering the behavior of Eq. (5) for very high values of p, r becomes equal to $n-m$, with n being the degree of $D_{(jf)}$ or the number of brackets in the denominator of Eq. (5). Thus n has to be at least $2+3=5$.

No more poles and zeros than those obtained by the above consideration were necessary to fit our experimental data. This was proved by enlarging n and m and watching whether this procedure improved the computer-aided approximation of the measured frequency responses.

The numerical determination of the n_i and τ_i in Eq. (5) had to be done by computers. At first the curve-fitting routine of Strobel (1968) was employed. However, this program had a tendency to fit experimental scatter by complex poles (or time constants). Thus Dr. Keunecke provided us with a modified version, in which the time constants were changed by small steps and the zeros were calculated by a least-squares fit routine. This program was used to improve the approximations gained by the routine of Strobel or to convert complex time constants into real ones, if they were heavily damped. It was found that in the case of our measurements the real time constants gave equally good or even better fits than the complex ones.

The philosophy of preferring real time-constants is as follows. Finding real time-constants is much more conservative than finding complex ones: as shown in the appendix of a preceding paper (Hansen, 1978), complex time constants point to the existence of a feed-back loop, whereas real ones do not exclude the existence of a feed-back loop. The transition from real τ_i to complex τ_i may be just a minor change in the loop amplification of the feed-back circuit. Whereas the false assumption of a real time constant results in a small numerical error, the incorrect assumption of complex time constants gives a basically wrong model. This problem occurs only if the complex time constants are heavily damped, i.e., if the real component is greater than the imaginary one.

The numerical values of the inverse zeros n_4 and n_5 and of the time constants obtained from 10 frequency responses are shown in Table 2. It is seen that the scatter of n_4 and of n_5 is large. This is the reason for the different types of frequency responses (*see* Fig. 3), as discussed below.

The electrical impedance of the plasma membrane resulting in a time constant between 0.1 and 0.01 sec is expected to show up in the frequency responses of the light-induced signals. Warncke (1974) has shown that his highest time constant of the light-induced signals coincides with the electrical time constants.

His result is verified by our measurements. In a separate batch of cells the electrical time constant of the plasma membrane was determined by injecting a current via a second microelectrode. Since the geometry of the current flow is similar to that caused by spot light, the cable properties need not to be considered. A mean value of 0.01 sec was found, corresponding to a cutoff frequency of 16 Hz. The mean value of τ_8 displayed in Table 2 is 0.0086 sec. Thus it is confirmed again that τ_8 originates from the electrical impedance of the membrane.

Discussion

The benefits of the employment of sine waves for the investigation of complicated systems is demonstrated again. Whereas in the preceding papers (Hansen, 1974; 1978) sine waves were used in order to check for the linearity of the system (*see* Fig. 2), in this paper the periodicity of sine waves is utilized for the application of filter- and correlation techniques. Thus the upper theoretical frequency limit of 20 Hz (*see Materials and Methods*) could be reached.

The new information gained by the extension of the frequency range is the existence and the numerical values of n_4, n_5, τ_6, τ_7, and τ_8.

The whole frequency response of the light-induced changes in the membrane potential in *Nitella* in the accessible range of frequencies from 6.7×10^{-5} to 20 Hz is obtained, if the results of the present investigation and of the preceding one (Hansen, 1978) are combined. The resulting transfer function is given by Eq. (6).

$$H_{(jf)} = H_o \frac{(1-pn_1)(1-pn_2)(1-pn_3)(1-pn_4)(1-pn_5)}{(1-p\tau_1)(1-p\tau_2)(1-p\tau_3)(1-p\tau_4)(1-p\tau_5)(1-p\tau_6)} \cdot \frac{1}{(1-p\tau_7)(1-p\tau_8)}. \tag{6}$$

The unit, μV/%, reflects the logarithmic dose-effect function of the light effect. The magnitude of the output signal depends on the modulation depth q [Eq. (3)] and not on the intensity i_m in Eq. (1) (Hansen & Gradmann, 1971; Hansen *et al.*, 1973). The values of H_o, of the n_i and of the τ_i are displayed in Table 3. Since the temperature in the present experiments was 25 to 27 °C, the data obtained by Hansen (1978) at 27 °C are used for Table 3.

τ_4 and τ_5 are provided by both investigations. In Table 3 it is seen that τ_4 is reproduced very well. The origin for the different values of τ_5 is

Table 3. A synopsis of the mean values of the kinetic data of Eq. (5), obtained from the measurements of Hansen (1978, 27 °C) (*A*) and from the present investigation (*B*)[a]

	τ_1	τ_2 and τ_3	τ_4	τ_5	τ_6	τ_7	τ_8
A	−315	−53+/−372*j*	−12	−2.5			
σ	4	2.1 1.6	1.5	1.6			
B			−10.2	−0.82	−0.19	−0.034	−0.0086
σ			1.7	1.2	1.9	2.0	4.3
	n_1	n_2 and n_3	n_4 and n_5		H_{dep}	H_s	
A	773	35+/−277*j*			63.5		
σ	3	3.5 1.5			1.5		
B			−0.03+/−0.074*j*			70	
σ			3.4	3.3		1.5	

[a] Light intensity 1 W/m^2, temperature 25 to 27 °C. The unit of the τ_i and of the n_i is sec. The unit of H_s and H_{dep} is μV/%modulation. The variance σ is given as a factor

unknown. However, it should be mentioned that the new measurements were made 3 years later than the old ones.

Creating a Model from a Measured Frequency Response

The relationship between frequency responses and biochemical reactions is demonstrated in *Appendix II* by means of two-step reactions which may stand for the upper and the lower pathway in Fig. 4.

There are two sorts of important parameters to deal with: the "poles" which are the roots of the denominator, and the "zeros" which are the roots of the numerator of the frequency responses like Eq. (6). In this article the usage of the "time constants" (τ_i), which are the inverse poles, and of the inverse zeros n_i, which will be called "zeros", too, is preferred.

From Eq. (6) we know that we have to deal with seven reactions labeled by the seven time constants τ_1 to τ_7. τ_8 is neglected, because it is known to originate from the electrical membrane impedance. The seven reactions have to be arranged in such a manner that the zeros n_1 to n_5 are created. The zeros contain the information about the arrangement of the reactions labeled by the time constants. Finding this structure is called the "inverse problem". Since different structures may result in the same transfer function, the inverse problem is ambiguous.

In *Appendix II* it is shown that zeros can be generated by the backflow from subsequent reaction chains [*see* Eq. (A19)] or by the

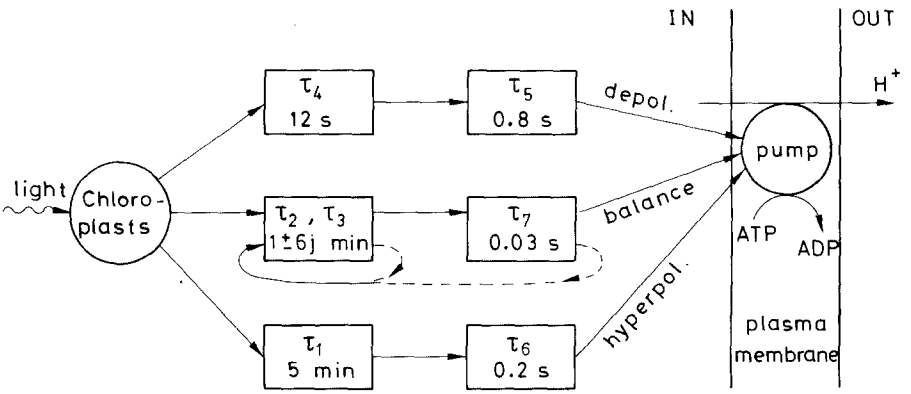

Fig. 4. The improved model of the arrangement of the reactions which mediate the light effect in *Nitella* on membrane potential. Both the depolarizing and the hyperpolarizing pathway may be embodied by two-step reactions of the type represented by Eqs. (A13) and (A22). The unknown reactions are labeled by the apparent time constants of Eqs. (6) and (7). For simplicity in displaying the physical relationships, the negative signs of the time constants have been omitted

superposition of the actions of parallel pathways. Since the backflow from subsequent reaction chains is not capable of creating zeros with positive real components [because these zeros are the poles of the subsequent chain, *see* Eqs. (A19) and (A21)], and since n_1 to n_5 all exhibit positive real components in some experiments (*see* Hansen, 1978, for n_1 to n_3, and Table 2 for n_4 and n_5), it is obvious that we have to deal with a parallel-pathway model.

The Model of the Action of Light on Membrane Potential

In Fig. 4 a model is shown which is an extension of the model proposed by Hansen (1978). It implies that light acts via three parallel pathways on the electrogenic pump at the plasma membrane. The involvement of the electrogenic pump has not been proved completely. However, from the comparison of the light-induced changes in potential and in resistance it is very likely (Hansen & Keunecke, 1977). The upper and the lower pathways are of the kind discussed in *Appendix II*. They consist of two reaction steps in series, which are labeled by the time constants τ_4, τ_5 and τ_1, τ_6, respectively. The upper quick depolarizing pathway slows down the pump with light, the lower slow hyperpolarizing pathway speeds up the pump with light. The medium pathway comprises

τ_7 and the conjugate complex time constants τ_2 and τ_3. Complex time-constants point to the existence of a feed-back loop (*see* appendix of Hansen, 1978).

It is assumed that these pathways are involved in the regulation of a relevant parameter in the cytoplasm, e.g., the pH value. This suggestion is supported by impedance measurements in the range of frequencies related to τ_2 and τ_3 (Hansen, 1978). The idea is as follows: a rough balance of the light-induced changes in pH is already provided by the action of the depolarizing pathway and by the action of the hyperpolarizing pathway. The medium pathway has to sense the result of it and to perform the final balance. This concept explains that the medium pathway is found to support sometimes the upper pathway and sometimes the lower one (*see* Hansen, 1978). This combination of forward-acting and of feed-back regulations seems to be a very powerful tool designed to prevent large perturbations of the controlled parameter (e.g., the pH), when the mode of metabolism is changed.

The Mathematical Procedure Related to the Creation of a Model

The curve-fitting routines deliver the frequency responses in the form of Eq. (6). Eq. (7) is mathematically identical to Eq. (6), but rearranged in such a manner that it reflects the basic features of the model shown in Fig. 4.

$$H_{(jf)} = H_{\mathrm{dep}} \left\{ \frac{1}{(1-p\tau_4)(1-p\tau_5)} + \frac{c_h}{(1-p\tau_1)(1-p\tau_6)} + \frac{c_c(1-pn)}{(1-p\tau_2)(1-p\tau_3)(1-p\tau_7)} \right\}. \tag{7}$$

The sum in the bracket corresponds to the superposition of the three pathways. Thus the terms in the bracket of Eq. (7) are the frequency responses of the isolated pathways. These isolated frequency responses are displayed in Fig. 5*A*.

The zeros n_1 to n_5 in Eq. (6) are replaced by the zero n, and the two splitting parameters c_h and c_c in Eq. (7). These splitting parameters c_h and c_c give the relative magnitudes of the effects of the hyperpolarizing and of the balancing pathway, respectively, at low frequencies compared with the quick depolarizing pathway which is standardized to "1".

Roughly speaking, the zeros are created at those frequencies where the amplitudes of the other two pathways approach the amplitude of the

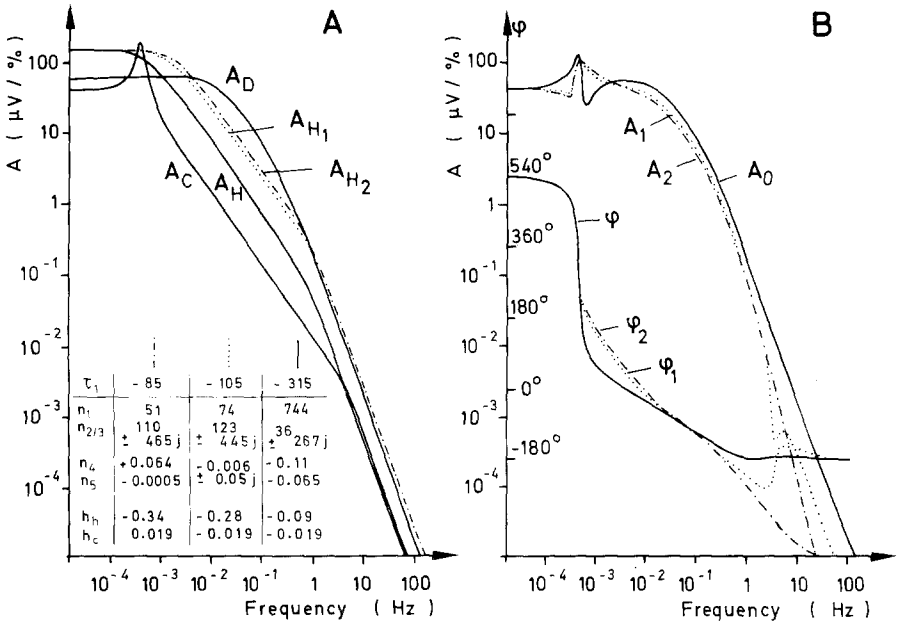

Fig. 5. The generation of the zeros from the superposition of the frequency responses of the isolated pathways of the model in Fig. 4. (*A*): The calculated frequency responses of the three isolated pathways. A_D, A_H and A_C are the frequency responses of the depolarizing, of the hyperpolarizing, and of the balancing (control) pathway, respectively, calculated from the corresponding terms in Eq. (7) by making use of the kinetic parameters displayed in Table 3 with the exception of τ_1, which is subjected to arbitrary changes. (*B*): The calculated frequency responses of the amplitudes and of the phases of the composite system, which result from the superposition of the isolated pathways shown in *A* according to Eq. (7). The smooth curves are calculated completely from the data of Table 3. The dotted lines demonstrate the influence of a shift in τ_1 from -315 to -105 sec (indexed by "1") and to -85 sec (indexed by "2"). The values of the zeros n_1 to n_5 (dimension: sec) of the curves in *B* which result from the superposition of the three pathways and the high frequency splitting parameters h_h and h_c [*see* Eqs. (11) and (12)] are given in the lower left corner of *A*. c_h and c_c were -2.4 and $+0.69$ for all curves. τ_2 to τ_7 are given in Table 3

strongest pathway. This happens at low frequencies resulting in n_1, n_2 and n_3. At medium frequencies the quick pathway is dominating. However, because τ_5 is slower than τ_6 and τ_7, the quick pathway bends to the $1/f^2$-slope earlier than the other two pathways (*see* the smooth lines in Fig. 5*A*). Thus the frequency responses of the amplitudes of the three pathways meet again at high frequencies and create n_4 and n_5.

The Origin of the Enormous Scatter in the Curve Shapes

The observed scatter (*see* Fig. 3 and Table 2) is an inherent feature of the mechanism of the generation of the zeros described above. To

illustrate the dependency of the curve shapes on the original parameters of the system, the frequency responses for different values of τ_1 have been calculated and are displayed in Fig. 5. The other parameters τ_2 to τ_7, c_c and c_h have been kept constant and are equal to the mean values displayed in Table 3. τ_1 has been selected for this demonstration because it is supposed to have brought about the changes in h_h, which is the critical parameter in Fig. 3 [*see* Eq. (11)]. The proposed changes in τ_1 from -315 to -85 sec are in line with the scatter factor of 4 given by σ in Table 3.

Assuming new values of τ_1 (-105 and -85 sec instead of -315 sec) causes a shift of the frequency responses of the hyperpolarizing pathway, A_{H1} and A_{H2}, towards higher frequencies (*see* Fig. 5*A*, dotted lines). The resulting composite frequency responses of the entire system in Fig. 4 (which are measured in an experiment) are affected by this shift in two regions: at low frequencies, where n_1, n_2 and n_3 are located, and at high frequencies, where n_4 and n_5 are found (*see* dotted lines in Fig. 5*B*).

In this paper we are interested in the high frequency region. We see that quite different types of frequency responses can be generated by the shift of the single parameter τ_1. In the case of the original data of Table 3, A_H and A_C (smooth lines in Fig. 5*A*) do not reach the depolarizing pathway A_D. Thus A_D is dominating in the whole high frequency region, and the $1/f^2$-slope is maintained. This is mathematically reflected by the location of n_4 and n_5 close to τ_6 and τ_7, which makes them nearly ineffective.

The notch displayed by No. 7 in Fig. 3 is obtained for $\tau_1 = -105$ sec. The small further step to $\tau_1 = -85$ sec results in the $1/f^3$-slope exhibited by No. 4 in Fig. 3.

The dotted frequency responses, A_1 and A_2, φ_1 and φ_2, in Fig. 5*B* demonstrate the necessity of extending the frequency range. In our earlier experiments there were no measurements at frequencies higher than 0.5 Hz.

Thus the observed frequency responses with an $1/f^3$-slope of the kind of A_1 or of A_2 led Hansen (1978) to the assumption that the light effect acts via pathways comprising three reaction steps. That was the reason that he located τ_5 and τ_6 in series. The present investigation has revealed the additional zeros n_4 and n_5. These zeros may happen to be placed at higher frequencies than τ_6. In this case τ_6 bends the resulting frequency reponse to the $1/f^3$-slope, before its effect is canceled by the zeros n_4 and n_5. By means of the new zeros, the $1/f^3$-slope is identified as the result of a superposition of two-step reactions as illustrated in Fig. 4.

A similar variety of curve shapes can be created by changing the other time constants or c_h and c_c. The essential feature is the crossing or not crossing of the isolated frequency responses A_D, A_C, and A_H.

A Test for the Model in Figure 4

When Hansen (1978) proposed the precursor of the model in Fig. 4, n_4 and n_5 were unknown. In that case it was no problem to calculate the three parameters n, c_n and c_c from the three measured zeros n_1 to n_3. However, now the five zeros n_1 to n_5 in Eq. (6) determine the same three parameters n, c_h and c_c in Eq. (7). The resulting set of five equations is only resolvable if two of the equations are dependent on the other three equations. This dependency has to result from the selected model and can be used as a test for the model, as will be shown below.

In the range of the frequencies related to τ_5 to τ_7, the frequency $f=p/2\pi j$ is so high that the "1" in the brackets $(1-p\tau_1)$, $(1-p\tau_2)$, $(1-p\tau_3)$, $(1-p\tau_4)$ and $(1-pn)$ of Eq. (7) may be omitted. This converts Eq. (7) to Eq. (8).

$$H_{(jf)}=H_o\left\{\frac{1}{p\tau_4(1-p\tau_5)}+\frac{c_h}{p\tau_1(1-p\tau_6)}+\frac{c_c pn}{p\tau_2\tau_3(1-p\tau_7)}\right\} \tag{8}$$

$$=\frac{H_o}{p\tau_4}\left\{\frac{1}{(1-p\tau_5)}+\frac{c_h\tau_4}{\tau_1}\cdot\frac{1}{(1-p\tau_6)}+\frac{c_c n\tau_4}{\tau_2\tau_3}\cdot\frac{1}{(1-p\tau_7)}\right\} \tag{9}$$

$$=\frac{H_o}{p\tau_4}\left\{\frac{1}{(1-p\tau_5)}+\frac{h_h}{(1-p\tau_6)}+\frac{h_c}{(1-p\tau_7)}\right\}. \tag{10}$$

In Eq. (10) the new splitting parameters h_h and h_c are introduced. Whereas c_h and c_c were measures of the relative magnitudes of the effects of the hyperpolarizing pathway and of the balancing one at low frequencies, h_h and h_c are the measures of the relative effects at high frequencies. The comparison of Eqs. (9) and (10) shows that the model in Fig. 4 implies the following relationships:

$$h_h=\frac{c_h\tau_4}{\tau_1}, \qquad h_c=\frac{c_c n\tau_4}{\tau_2\tau_3}. \tag{11), (12}$$

The experimental data of this investigation were fitted by Eq. (5), because there were no measurements at low frequencies. The application of the above consideration for high frequencies converts Eq. (5) to Eq. (13).

$$H_{(jf)}=\frac{H_s}{p\tau_4}\cdot\frac{(1-pn_4)(1-pn_5)}{(1-p\tau_5)(1-p\tau_6)(1-p\tau_7)}. \tag{13}$$

As discussed above, the zeros n_4 and n_5 are created by the superposition of the three pathways, if the model in Fig. 4 is correct. To test this assumption, we split Eq. (13) into three terms like Eq. (10).

$$H_{(jf)}=\frac{H_s}{p\tau_4}\left\{\frac{1}{(1-p\tau_5)}+\frac{h_h}{(1-p\tau_6)}+\frac{h_c}{(1-p\tau_7)}\right\}. \tag{14}$$

The comparison of Eqs. (13) and (14) shows that the h_h and the h_c of Eq. (14) can be calculated from the following set of equations:

$$\tau_6+\tau_7-n_4-n_5+h_h(\tau_5+\tau_7-n_4-n_5)+h_c(\tau_5+\tau_6-n_4-n_5)=0 \tag{15}$$

$$\tau_6\tau_7-n_4n_5+h_h(\tau_5\tau_7-n_4n_5)+h_c(\tau_5\tau_6-n_4n_5)=0. \tag{16}$$

In Table 2 the splitting parameters h_h and h_c calculated from the kinetic data of the 10 displayed frequency responses by means of Eqs. (15) and (16) are shown.

This survey is given to demonstrate one of the benefits of the model in Fig. 4: The numerical values of h_h and of h_c verify that the model is a good one, because it is capable of reducing the great variability of the measured frequency responses (*see* Fig. 3) to much smaller changes in two basic coefficients, namely, h_c and h_h.

The most important feature, however, is that h_h and h_c can be determined by two independent ways, from the high frequency data by means of Eqs. (15) and (16), and from the low-frequency data by means of Eqs. (11) and (12). The values obtained by the first method will be called the "measured values", the other ones the "predicted values".

Since we have no measurements which span the whole frequency range from 1 cycle/4 hr to 20 Hz (this curve-fitting routine exceeds the range of available real numbers in a PDP 10) the original data of Hansen (1978) and of Korff (1979) were used in order to calculate h_h and h_c by means of Eqs. (11) and (12). The averaged values are displayed in Table 4 and can be compared with the measured values shown in the first column of Table 4.

From Table 4 it is seen that the predicted values of h_h and h_c indeed coincide with the measured values within the limits of experimental scatter. The measured value of $h_h=0.3$ is just the mean value of the predicted ones of Hansen and of Korff. (There seems to be a historical development in h_h: 1974, 0.1; 1976, 0.3; 1978, 0.5.) The coincidence may not be expected to be better, because not only experimental scatter but also system-inherent deviations may be involved.

A major point regarding this problem is the question whether a τ_i in Eq. (6) represents a single time constant or the center of a distribution of time

Table 4. Comparison of the measured values of h_h and h_c [Eqs. (15) and (16)] with the predicted values [Eqs. (11) and (12)] obtained from the low-frequency measurements of Hansen (1978) and of Korff (1979)[a]

	Measured (*see* Table 2)	Predicted coefficients [Eqs. (11) and (12)]			
		Data of Hansen (1978)			Data of Korff (1979)
		7 °C	17 °C	27 °C	
h_h	−0.31	−0.15	−0.11	−0.10	−0.51
σ	1.8	2.7	2.2	2.6	1.7
h_c	0.035	0.028	0.019	0.019	0.008
σ	4.0	3.3	3.4	2.4	5.0
neg. h_c	10 %	30 %	25 %	50 %	15 %

[a] "neg. h_c" gives the percentage of negative values of h_c.

constants. The phase shifts caused by such an ensemble of time constants may be a little different from the phase shifts caused by a single time constant, thus resulting in slightly different zeros and slightly different h_h and h_c. However, a treatment of this problem provides insurmountable mathematical difficulties.

H_s is not discussed, since the experimental data were fitted by means of Eq. (5). Since H_{dep} in Eq. (6) is related to the fast depolarizing pathway, it should be equal to H_s (*see* Eq. (14) and Table 3).

Besides the numerical values of h_h and h_c, other features, too, support the model in Fig. 4. The scatter of the predicted values of h_h and h_c correspond to the scatter of the measured values. Even the number of negative signs of c_c is reproduced to some extent.

The tremendous scatter of h_c or c_c is believed to originate from the special function of this pathway as a control unit (*see* Hansen, 1978, and the discussion above).

These investigations have been supported by the Deutsche Forschungsgemeinschaft. We are indebted to Dr. P. Keunecke for allowing us to use his curve-fitting routine, and to Prof. Dr. C.L. Slayman and Dr. D. Sanders, New Haven, for helpful discussions. All computations were done on the PDP 10 of the Kieler Rechenzentrum.

Appendix I

Determining the Amplitude and Phase-Shifts of Noisy Signals by Means of Cross Correlation

The technique of cross correlation. $I_0 \sin \omega t$ is the signal modulating the light intensity [Eq. (1)]. At the plasma membrane it induces the sinusoidal

signal

$$u = A_o \sin(\omega t + \varphi). \tag{A1}$$

Because it is superposed by the noise $n_{(t)}$, the microelectrode records

$$v_{(t)} = A_o \sin(\omega t + \varphi) + n_{(t)}. \tag{A2}$$

By means of the correlator $v_{(t)}$ is multiplied with $I_o \sin \omega t$ and the product is integrated over time.

$$M_o = \frac{1}{T} \int_0^T \{I_o A_o \sin(\omega t + \varphi) \sin \omega t + I_o n_{(t)} \sin \omega t\}\, dt \tag{A3}$$

$$= I_o A_o \cos \varphi + \overline{I_o n_{(t)} \sin \omega t}. \tag{A4}$$

Since the noise $n_{(t)}$ and the light signal $i_{(t)}$ are not correlated, the second term of Eq. (A4) has to vanish, if the integration time is long enough.

To determine A_o and φ separately, a second correlator has to be used with the reference signal $I_o \cos \omega t$ delayed by 90°.

$$M_{90} = I_o A_o \sin \varphi. \tag{A5}$$

Equations (A4) and (A5) lead to

$$A_o = (M_o^2 + M_{90}^2)/I_o \tag{A6}$$

$$\varphi = \arctan \frac{M_{90}}{M_o}. \tag{A7}$$

The required correlation time T. The required correlation time T [*see* Eq. (A3)] depends on the signal to noise ratio Q desired at the output of the correlator, and on the magnitude of the input signal A_o compared with $D_{(n)}$, the measure of the noise (Charkewitsch, 1968).

$$T^2 = \frac{Q D_{(n)}}{A_o^2}. \tag{A8}$$

Since we are interested in a lower limit for T, it is sufficient to use the rough estimation

$$D_{(n)} = T \tau_o p n_{(f)}. \tag{A9}$$

The time constant of internal correlation, τ_o, is given by the bandwidth of the filter Δf

$$\tau_0 = 1/\Delta f \tag{A10}$$

and

$$pn_{(f)} = sn_{(f)}\,\Delta f. \tag{A11}$$

$sn_{(f)}$ is the spectral density of the noise.

Equations (A8) to (A11) lead to

$$T = \frac{Q\,sn_{(f)}}{A_o^2}. \tag{A12}$$

Appendix II

The Relationship Between the Kinetics of Chemical Reactions and Frequency Responses

The description of the temporal behavior of chemical reactions in terms of frequency responses will be demonstrated by means of an example which may stand for the hyperpolarizing and the depolarizing pathway of light action in the model of Fig. 4.

Since we restrict our investigations to the range of linear responses (*see* Fig. 2), we may treat the following reactions as pseudo-first-order reactions. The concentrations of other reactants are included in the rate contants k_i (Eigen, 1968; Bernasconi, 1976). Thus a two-step reaction like the upper or lower pathway in Fig. 4 is represented by Eq. (A13).

$$I \underset{k_{-1}}{\overset{k_o}{\rightleftharpoons}} A \underset{k_{-2}}{\overset{k_1}{\rightleftharpoons}} B \xrightarrow{k_2}. \tag{A13}$$

The light intensity I generates A, which converts into B. B decays. Equation (A13) leads to the following rate equations

$$\frac{da}{dt} = k_o i - (k_{-1} + k_1)\,a + k_{-2}\,b \tag{A14}$$

$$\frac{db}{dt} = k_1 a - (k_{-2} + k_2)\,b. \tag{A15}$$

The small letters i, a, b represent the time-courses of I and of the concentrations of A and B.

The frequency responses like Eq. (5) or Eq. (6) are obtained, if the above differential equations are solved for a sinusoidal input signal as it is given by Eq. (1). The mathematics become simpler, if the complex exponential functions are used. Using this presentation Eq. (1) converts to

$$i_{(t)} = i_m + I e^{pt} \tag{A16}$$

with $p = 2\pi jf$, $j = \sqrt{-1}$, f being the frequency. This results in sinusoidal changes of the concentrations a and b of the reactants A and B in Eq. (A13)

$$a_{(t)} = a_m + A e^{pt} \quad \text{and} \quad b_{(t)} = b_m + B e^{pt}. \tag{A17a, b}$$

A and B in Eqs. (A17a) and (A17b) should be distinguished from the chemical symbols A and B in Eq. (A13). Like I, they are complex amplitudes, comprising the value of the amplitude, indexed by zero [*see* I_o in Eq. (1)] and the phase shift φ, e.g., in the case of A

$$A = A_o e^{j\varphi}. \tag{A18}$$

Inserting Eqs. (A16) and (A17a, b) into Eqs. (A14) and (A15) results in the so-called transfer functions or frequency responses given by Eqs. (A19) to (A21). The terms comprising only the mean values i_m, a_m, and b_m cancel each other due to the steady-state condition.

$$\frac{A}{I} = \frac{k_o(p + k_{-2} + k_2)}{(p + k_{-2} + k_2)(p + k_{-1} + k_1) - k_1 k_{-2}} \tag{A19}$$

$$\frac{B}{I} = \frac{k_o k_1}{(p + k_{-2} + k_2)(p + k_{-1} + k_1) - k_1 k_{-2}} \tag{A20}$$

$$\frac{B}{A} = \frac{k_1}{(p + k_{-2} + k_2)}. \tag{A21}$$

The time constants. The roots of the denominator are called the "poles"; the roots of the numerator are called the "zeros". In this article we use the inverse poles, because they are the apparent time constants of the reaction steps and the inverse zeros, which will be called "zeros", too.

A transfer function having 8 time constants like that one measured in *Nitella* [Eq. (6)] can be generated by a chain of 8 reaction steps in series. However, such a chain cannot create all essential features of Eq. (6).

At first, there are the complex time constants τ_2 and τ_3 which implement the involvement of a feed-back loop (*see* appendix of Hansen, 1978). The major problem, however, is given by the zeros. Zeros result from arrangement of the reaction steps.

The creation of zeros. In the example of Eq. (A19) the zero is generated by the backward reaction related to k_{-2}. These zeros must have negative real components, since they are equal to the poles of the subsequent chain [*compare* Eqs. (A19) and (A21)], and poles may never have positive real components, otherwise the system becomes unstable.

In our experiments, n_4 and n_5 sometimes have positive real components (*see* Table 2). Zeros of every kind can be delivered by parallel pathways. Let us assume that light I acts via two chains of the type represented by Eq. (A13) on the electrogenic pump P.

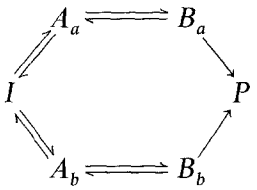

(A22)

The activity of the pump can be defined by

$$P = B_a + \alpha B_b. \tag{A23}$$

Calculating the roots p_1 and p_2 of the denominator converts Eq. (A20) to Eq. (A24)

$$\frac{B}{I} = \frac{c^*}{(p-p_1)(p-p_2)} = \frac{c}{(1-p\tau_1)(1-p\tau_2)}. \tag{A24}$$

Using this form for the transfer functions B_a/I and B_b/I results in:

$$\frac{P}{I} = \frac{B_a}{I} + \alpha\frac{B_b}{I} \tag{A25}$$

$$= \frac{c_a}{(1-p\tau_{1a})(1-p\tau_{2a})} + \alpha\frac{c_b}{(1-p\tau_{1b})(1-p\tau_{2b})} \tag{A26}$$

$$= \frac{H_{ab}(1-pn_c)(1-pn_d)}{(1-p\tau_{1a})(1-p\tau_{2a})(1-p\tau_{1b})(1-p\tau_{2b})} \tag{A27}$$

with

$$n_c, n_d = \frac{\tau_{1b}+\tau_{2b}+\beta\tau_{1a}+\beta\tau_{2a}}{2(\tau_{1b}\tau_{2b}+\beta\tau_{1a}\tau_{2a})} \pm \sqrt{(\;)^2 - \frac{1+\beta}{\tau_{1b}\tau_{2b}+\beta\tau_{1a}\tau_{2a}}}. \tag{A28}$$

The bracket in the root stands for the term in front of the root. The amplification factors in the numerators of Eq. (A24) to Eq. (A27) are of minor interest and are not given explicitly.

From Eq. (A28) it is seen that the inverse zeros n_c and n_d can accept any real or complex value by changing $\beta = \alpha c_b/c_a$. Thus the parallel pathway model is the most effective way of creating the wanted zeros.

References

Bernasconi, C. F. 1976. Relaxation Kinetics. Academic Press, New York-San Francisco-London

Charkewitsch, A. A. 1968. Signale und Störungen. pp. 74–82 and 272–274. Oldenburg-Verlag. Munich-Vienna

Eigen, M. 1968. New looks and outlooks on physical enzymology. *Q. Rev. Biophys.* **1(1)**: 3

Forsberg, C. 1965. Nutritional studies of *Chara* in axenic cultures. *Physiol. Plant* **18**: 275

Grahn, J. 1978. On-line Messung des *1/f*-Rauschens der Membranspannung in *Nitella* mit Hilfe digitaler Filter und Autokorrelationsfunktionen auf einem Mikrocomputer. Diplom-thesis. University of Kiel, Kiel

Hansen, U.-P. 1970. Ein digitaler Sinusgenerator für sehr lange Periodendauern. *Elektronik* **19**: 221

Hansen, U.-P. 1974. Preliminary results of an approach to the quantitative description of the action of light on the membrane potential of *Nitella*. *In:* Membrane Transport in Plants. U. Zimmermann and J. Dainty, editors. pp. 139–145. Springer-Verlag, Berlin-Heidelberg-New York

Hansen, U.-P. 1978. Do the light-induced changes in the membrane potential of *Nitella* reflect the feed-back regulation of a cytoplasmic parameter? *J. Membrane Biol.* **41**: 197

Hansen, U.-P., Gradmann, D. 1971. The action of sinusoidally modulated light on the membrane potential of *Acetabularia*. *Plant Cell Physiol.* **12**: 335

Hansen, U.-P., Keunecke, P. 1977. Parallel pathways in the action of light on membrane potential in *Nitella*. *In:* Transmembrane Ionic Exchanges in Plants. M. Thellier, A. Monnier, M. Demarty, and J. Dainty, editors. pp. 333–340. C.N.R.S., Rouen/Paris

Hansen, U.-P., Warncke, J., Keunecke, P. 1973. Photoelectric effects in *Characean* cells. I. The influence of light intensity. *Biophysik* **9**: 197

Korff, H.-M. 1979. Untersuchungen zur Analyse eines biologischen Informationsübertragungssystems mit stochastischen Testsignalen. Ph. D. Thesis, University of Kiel, Kiel

Strobel, H. 1968. Systemanalyse mit determinierten Testsignalen. VEB-Verlag Technik, Berlin

Warncke, J. 1974. *1/f*-Rauschen des Membranpotentials von *Nitella* und sein Einfluß auf die Lichtantwort. *Ber. Dtsch. Bot. Ges.* **87**: 537